

FIG. 2. FDCD and negative capacitance were observed in both the (a) C - V profile and (b) C - f profile of the n^+ -GaN/ $\text{Al}_{0.026}\text{Ga}_{0.974}\text{N}$ structure (sample 1158). From the C - f profile, inverse relaxation times of approximately 1.77 ± 0.05 and 155 ± 9 μs were calculated from the points where the capacitance transitioned from negative to positive or from positive to negative. The inset shows a C - f profile of the n^+ -GaN/ $\text{Al}_{0.1}\text{Ga}_{0.9}\text{N}$ structure (sample 1547).

Mott transition in GaN ($\sim 8 \times 10^{17} \text{ cm}^{-3}$). Thus, the n^+ -GaN/ $\text{Al}_{0.026}\text{Ga}_{0.974}\text{N}$ interface is analogous to a metal-semiconductor interface.

Using dry etching techniques, the structures were processed to form square mesas with the areas inside the metal rectangular contact fully etched. However, the n^+ -GaN layer under the rectangular contact remained intact ($0.2 \mu\text{m}$ thick), thus, a small n^+ -GaN/ $\text{Al}_{0.026}\text{Ga}_{0.974}\text{N}$ heterojunction would still be present at the top-contact/barrier interface. The UV/IR dual-band detector operates by collecting carriers from both intraband IR transitions in the n^+ -GaN emitter layer and interband UV transitions in the $\text{Al}_{0.026}\text{Ga}_{0.974}\text{N}$ barrier layer, as discussed in detail elsewhere.⁵ Etching the top-contact emitter will drastically reduce the IR active region of the sample; however, the n^+ -GaN layer under the rectangular contact will remain intact between the metal contact and the $\text{Al}_{0.026}\text{Ga}_{0.974}\text{N}$ barrier.

C - V and C - f measurements were carried out using a computer-controlled Hewlett-Packard 4284A LCR meter. C - V scans were taken from -2 to $+2$ V with a 50 mV step width and sine output amplitude set at 5 mV from 100 Hz to 1 MHz, while the C - f scans were taken between 1 kHz and 1 MHz. When forward biased, the top-contact was positive and the bottom-contact was negative. Under reverse bias, the top-contact was negative and the bottom-contact was positive. Different aspects of the electrical behavior can be studied using C - V and C - f characteristics. The applied voltage can either be held constant, and the ac frequency varied or the frequency can be held constant and the applied voltage varied. In the C - V profiles (see Fig. 2), negative capacitance was observed at frequencies of 10–500 kHz, which falls in the range of ~ 6 –600 kHz where negative capacitance occurred in the C - f profiles.

III. RESULTS AND DISCUSSION

When described in terms of charge accumulation at an interface, the capacitance is defined in terms of electrostatics,

$$C_0 = \frac{\epsilon \epsilon_0 A}{L}, \quad (1)$$

where ϵ is the relative dielectric permittivity, ϵ_0 is the dielectric permittivity in a vacuum, A is the mesa area, and L is the thickness of the barrier layer. However, this description can

only result in positive capacitance, as the total electric current is due solely to the displacement current and there is no contribution from a conduction current. Only in specific cases (high frequency or low temperature) can the capacitance be described by the electrostatic approximation, referred to as the geometric capacitance C_0 . The geometric capacitance for a $600 \times 600 \mu\text{m}^2$ mesa area is ~ 2.9 pF.

In order to describe the negative capacitance in terms of transient currents⁷, capacitance must be defined in terms of the imaginary part of the total admittance $Y(\omega)$,

$$C(\omega) = \frac{1}{\omega} \text{Im}[Y(\omega)] = \frac{1}{\Delta V} \int_0^\infty \delta J(t) \cos(\omega t) dt. \quad (2)$$

When the transient current $J(t)$, transient relaxation current $\delta j(t)$, and geometric capacitance C_0 are included, the capacitance is described⁷ by

$$C(\omega) = C_0 + \frac{1}{\omega \Delta V} \int_0^\infty \frac{-d\delta j(t)}{dt} \sin(\omega t) dt. \quad (3)$$

In Eq. (3), the sign of the second term is dependent on both the frequency and the behavior of the transient relaxation current in the time domain, specifically, the time derivative. In response to a small voltage step ΔV , if $\delta j(t)$ exhibits a positive-valued behavior (as reported⁷ in cases of impact ionization of impurities and other interface effects) and the magnitude is greater than C_0 , then the integral in Eq. (3) will become negative, resulting in a negative capacitance.

Frequency-dependent capacitance dispersion (FDCD) was observed in the C - V profiles, as shown in Fig. 2(a), and has been attributed to the presence of frequency-dependent trap states. Such phenomena have been observed in the 10 kHz–1 MHz regions of other GaN/AlGaIn heterojunctions such as Schottky diodes⁸ and heterojunction field effect transistors.⁹ In addition to FDCD, negative capacitance was observed in the C - V profiles of the n^+ -GaN/ $\text{Al}_{0.026}\text{Ga}_{0.974}\text{N}$ samples for frequency values of 10, 100, and 500 kHz. Negative capacitance has been observed in various other detector structures.^{6,10,11} The phenomenon has been attributed to carrier generation and recombination at interface states, most likely due to the presence of occupied trap states at the emitter-intrinsic layer interface.⁶ Due to the symmetry in the C - V profiles for both forward and reverse biasing, it is assumed that the processes responsible for negative capacitance and FDCD are present at both heterointerfaces.

The band diagram, including the location of the defect states under zero bias (in addition to the detection mechanism), is shown in Fig. 3(a). In the figure, the n^+ -GaN top-contact is to the left of the intrinsic $\text{Al}_{0.026}\text{Ga}_{0.974}\text{N}$ barrier layer and the n^+ -GaN bottom-contact is to the right; the diagram is intended to show the area between metal contacts. When a bias is applied across the device, as shown in Fig. 3(b), electrons with sufficient energy will either surmount the barrier or fill up any available trap states at the emitter-barrier interface. However, under certain frequency and bias conditions, electrons that possess sufficient energy will be able to dislocate any electrons already present in trap states below the Fermi level in a process similar to impact ioniza-

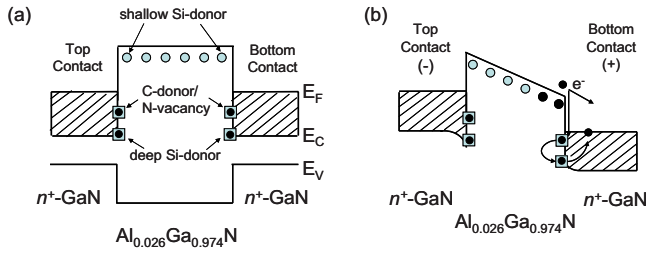


FIG. 3. (Color online) (a) The band diagram showing the location of defect energy states of the n^+ -GaN/ $\text{Al}_{0.026}\text{Ga}_{0.974}\text{N}$ detector structure under zero bias. (b) Schematic showing the mechanism leading to negative capacitance (with no external radiation). When the sample was reverse biased (top-contact is to the left of the barrier, bottom-contact to the right), electrons with sufficient energy were able to initiate an impact ionizationlike process by dislocating filled electron recombination centers below the Fermi level at the heterointerface.

tion or the Auger effect. These ionized trap states then act as electron recombination centers. In a n^+ -doped semiconductor, the relaxation times of electron recombination centers below the Fermi level are faster than those of the trap states above the Fermi level due to the excess of available electrons. When the electron occupancy of states below the Fermi level exceeds the occupancy of electrons above the Fermi level, the interface charge density variation is reversed and the capacitance becomes negative.

The negative capacitance observed in the C - f profiles, as seen in Fig. 2(b), allowed for the extrapolation of trap state relaxation times. The transitions from positive to negative capacitance occurred around 6 kHz, while the transition from negative to positive capacitance was at ~ 600 kHz. These two frequencies correlate with f^{-1} relaxation times of 155 ± 9 and $1.77 \pm 0.05 \mu\text{s}$, respectively. The faster relaxation time can be attributed to trap states below the Fermi level, possibly C-donor/N-vacancy and deep Si-donor defect states (pinned to the n^+ -GaN emitter layer), and the slower relaxation time to trap states above the Fermi level is probably due to shallow Si-donor states in the $\text{Al}_{0.026}\text{Ga}_{0.974}\text{N}$ barrier layer. At frequencies less than 6 kHz, both generation and recombination processes occur; however, the dominant trap states (shallow Si-donor) are located above the Fermi level and, consequently, the capacitance is positive. At ~ 6 kHz the trap states associated with a long relaxation time (slow trap states) are saturated and the electron recombination centers exhibiting short relaxation times (fast trap states) become dominant, thus, producing a negative capacitance. The fast trap states remain active until ~ 600 kHz, above which these trap states also become saturated. Once both generation and recombination processes have become inactive, due to high frequency, the capacitance returned to a positive value and approached the geometrical capacitance of the sample.

In order to model the C - f curves, the contributions from both majority and minority carriers are incorporated by including⁷ both positive and negative exponential components into the transient response current. The corresponding capacitance calculated from Eq. (3) is then

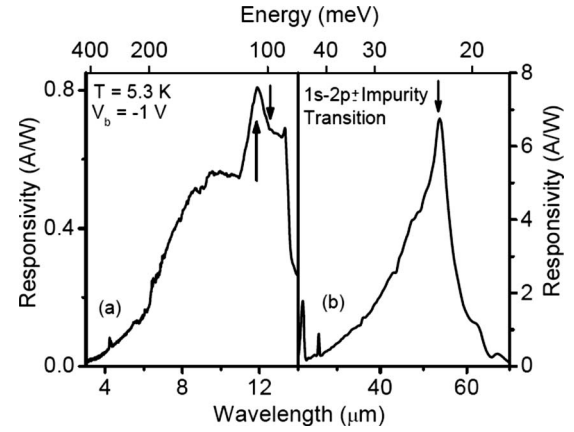


FIG. 4. (a) IR spectra showing two impurity related absorption centers with transitional energies of 93.4 ± 0.5 and 105 ± 1.5 meV, corresponding to activation energies of 125 ± 1 and 140 ± 2 meV. These absorption centers were attributed to N-vacancy/C-donor and deep Si-donor defect states, respectively. (b) A third absorption center was observed in the IR spectra with a $1s$ - $2p$ transitional energy of 23.1 ± 0.1 meV. This absorption center was attributed to shallow Si-donor impurities in the $\text{Al}_{0.026}\text{Ga}_{0.974}\text{N}$ barrier layer with an activation energy of 30.8 ± 0.2 meV.

$$C(\omega) = C_0 + \frac{a_1 \tau_1}{1 + (\omega \tau_1)^2} - \frac{a_2 \tau_2}{1 + (\omega \tau_2)^2}, \quad (4)$$

where a_1 and a_2 are constants and τ_1 and τ_2 are the relaxation times of the majority and minority carriers, respectively. Relaxation times $\tau_1 = 140 \pm 20 \mu\text{s}$ and $\tau_2 = 1.74 \pm 0.10 \mu\text{s}$ were found using Eq. (4) and were in agreement with the f^{-1} relaxation times from the C - f profiles. However, the amplitude of the C - f profiles could not be fitted using a Debye relaxation model, indicating that non-Debye processes are active in the sample. In the high-frequency limit ($\omega \rightarrow \infty$), the capacitance will approach the geometric capacitance of the sample due to finite inertia of the carrier transport processes when both the faster and slower traps can no longer respond.

The broad peak response peak observed in the IR spectra (see Fig. 4) between 8 and 14 μm is due to free carrier absorption. However, absorption peaks related to impurity transitions are observed superimposed on the free carrier response between 11 and 13.6 μm . Based on previous reports,¹²⁻¹⁴ the three impurity related absorption peaks were attributed to shallow Si-donor impurities in the $\text{Al}_{0.026}\text{Ga}_{0.974}\text{N}$ barrier layer with a $1s$ - $2p$ transitional energy of 23.1 ± 0.1 meV, which corresponds to an activation energy of 30.8 ± 0.2 meV. C-donor and/or N-vacancy impurities were attributed to the transitional energy of approximately 93.4 ± 0.5 meV, which correspond to an activation energy of 125 ± 1 meV. The third peak with a transitional energy of 105 ± 1.5 meV and activation energy of 140 ± 2 meV is attributed to Si-donor impurities at the heterointerface, which are pinned to the impurity band in the n^+ -GaN emitter layer. The conduction band offset of the n^+ -GaN/ AlGaIn heterointerface was calculated to be 137 ± 7 meV, which is consistent with the activation energy of 140 ± 2 meV.

To confirm that the negative capacitance displayed by the n^+ -GaN/ $\text{Al}_{0.026}\text{Ga}_{0.974}\text{N}$ sample was due to the presence of C-donor/N-vacancy and deep Si-donor defect states below

TABLE I. Summary of the experimentally obtained parameters and corresponding defect states. The activation energies were calculated from IR spectra transitional energies. Because the states below the Fermi level behave as a single trap state, the relaxation times are the same. The conduction band offset due to shallow Si-donor states (pinned to the n^+ -GaN emitter) was calculated to be 137 ± 7 meV.

Impurity	Position	Optical $E_{\text{activation}}$ (meV)	Relaxation times (μs)	
			Expt.	Calc.
Shallow Si-donor	Above E_F (pinned to AlGaN)	30.8 ± 0.2	155 ± 9	140 ± 20
C-donor/N-vacancy	States below E_F	125 ± 1	1.77 ± 0.05	1.74 ± 0.10
Deep Si-donor	States below E_F (pinned to GaN)	140 ± 2	1.77 ± 0.05	1.74 ± 0.10

the Fermi level, and not the shallow Si-donor states in the $\text{Al}_{0.026}\text{Ga}_{0.974}\text{N}$ barrier layer, a similar n^+ -GaN/ $\text{Al}_{0.1}\text{Ga}_{0.9}\text{N}$ structure (sample 1547) was used to obtain thermal activation energies. The n^+ -GaN/ $\text{Al}_{0.1}\text{Ga}_{0.9}\text{N}$ structure had the same Si doping concentration ($5 \times 10^{18} \text{ cm}^{-3}$) and shallow Si-donor activation energy (from IR spectra) as the n^+ -GaN/ $\text{Al}_{0.026}\text{Ga}_{0.974}\text{N}$ structure, but did not exhibit negative capacitance as the position of the C-donor and N-vacancy defect states were above the Fermi level due to an increased Al fraction.¹⁵ For comparison, a C - f profile from the n^+ -GaN/ $\text{Al}_{0.1}\text{Ga}_{0.9}\text{N}$ sample is provided in the inset of Fig. 2(b). Thus, an Arrhenius plot could be constructed using C - f relaxation times at temperatures ranging from 50 to 166 K and a thermal activation energy of 15 ± 1 meV was obtained for the n^+ -GaN/ $\text{Al}_{0.1}\text{Ga}_{0.9}\text{N}$ structure. Other groups reported¹⁶ similar thermal activation energies of 12–17 meV for shallow Si-donor impurities in GaN structures.

The energy difference of approximately 16 ± 1 meV between the activation energy estimated by IR spectroscopy and the thermal activation energy obtained from the Arrhenius plot indicates that the shallow Si-donors contribute to carrier transport through both thermionic emission and thermally assisted tunneling due to barrier thinning. The discrepancy between these two activation energy values is due to the fact that an Arrhenius plot provided the thermal activation energy required for the particle to reach an excited bound-state energy level where thermally assisted tunneling could take place through the potential barrier. In the case of thermally assisted tunneling, the activation energies obtained by an Arrhenius plot will therefore be lower than the activation energies obtained by IR spectroscopy, as observed here.

Combining the present experimental data, summarized in Table I, a comprehensive model including impurity trap states for n^+ -GaN/ $\text{Al}_{0.026}\text{Ga}_{0.974}\text{N}$ heterostructure can be constructed. The fast trap states are tentatively assigned to C-donor/N-vacancy and deep Si-donor defect states at the heterointerface positioned below the Fermi level, while the slow trap states appear to be correlated with shallow Si-donor impurities in the barrier layer positioned above the Fermi level. C-donor and N-vacancy related impurities are known to be incorporated into the material from the utilized organic precursors,⁵ such as the trimethylgallium (TMGa) or trimethylaluminum (TMAI) used as the Ga and Al precursors, respectively, and defects in the crystalline structure. Si-

donor related impurities are due to dopant migration from the top- (or bottom-) contact layers. The concentration of Si-donor traps have been found to correlate with Si-dopant incorporation during the growth process.¹⁶

IV. CONCLUSION

In summary, using C - V and C - f characterizations, negative capacitance and FDCD of n^+ -GaN/ $\text{Al}_{0.026}\text{Ga}_{0.974}\text{N}$ heterostructures were analyzed. Using both IR spectroscopy and thermal activation energies, the fast trap states are attributed to deep Si-donor and C-donor/N-vacancy defect states located at the n^+ -GaN/ $\text{Al}_{0.026}\text{Ga}_{0.974}\text{N}$ heterointerface with activation energies of approximately 140 ± 2 and 125 ± 1 meV, respectively; and the slow trap states are attributed to shallow Si-donor states located in the $\text{Al}_{0.026}\text{Ga}_{0.974}\text{N}$ barrier layer at the heterointerface with an activation energy of 30.8 ± 0.2 meV and a thermal activation energy of 15 ± 1 meV. Calculated (140 ± 20 and $1.74 \pm 0.10 \mu\text{s}$) and f^1 (155 ± 9 and $1.77 \pm 0.05 \mu\text{s}$) relaxation times were consistent to within the degree of uncertainty, with the f^1 relaxation times having a smaller uncertainty owing to the electron recombination center's non-Debye relaxation mechanism. Although multiple methods of determining activation energies allow for the identification of impurity traps, the additional use of C - V and C - f measurements provides information about the effects these trap states have on the electronic and optical properties of n^+ -GaN/ $\text{Al}_x\text{Ga}_{1-x}\text{N}$ detectors.

ACKNOWLEDGMENTS

This research was supported in part by the US Air Force under Small Business Innovation Research Program (SBIR) Contract No. FA9453-06-C-005, the Georgia Research Alliance, and GSU MBDAF. The authors would like to acknowledge Dr. Dave Cardimona and Dr. Bill Glass for fruitful discussions.

¹E. Munoz, E. Monroy, J. L. Pau, F. Calle, F. Omnes, and P. Gibart, *J. Phys.: Condens. Matter* **13**, 7115 (2001).

²M. P. Touse, G. Karunasiri, K. R. Lantz, H. Li, and T. Mei, *Appl. Phys. Lett.* **86**, 093501 (2005).

³J. Li, K. K. Choi, and D. C. Tsui, *Appl. Phys. Lett.* **86**, 211114 (2005).

⁴M. B. M. Rinzan, A. G. U. Perera, S. G. Matsik, H. C. Liu, Z. R. Wasilewski, and M. Buchanan, *Appl. Phys. Lett.* **86**, 071112 (2005).

⁵G. Ariyawansa, M. B. M. Rinzan, M. Alevli, M. Strassburg, N. Dietz, A. G. U. Perera, S. G. Matsik, A. Asghar, I. T. Ferguson, H. Luo, A. Bez-

- inger, and H. C. Liu, *Appl. Phys. Lett.* **89**, 091113 (2006).
- ⁶A. G. U. Perera, W. Z. Shen, M. Ershov, H. C. Liu, M. Buchanan, and W. J. Schaff, *Appl. Phys. Lett.* **74**, 3167 (1999).
- ⁷M. Ershov, H. C. Liu, L. Li, M. Buchanan, Z. R. Wasilewski, and V. Ryzhii, *IEEE Trans. Electron Devices* **45**, 2196 (1998).
- ⁸R. M. Chu, Y. G. Zhou, K. J. Chen, and K. M. Lau, *Phys. Status Solidi C* **0**, 2400 (2003).
- ⁹W. L. Liu, Y. L. Chen, A. A. Balandin, and K. L. Wang, *J. Nanoelectron. Optoelectron.* **1**, 258 (2006).
- ¹⁰M. Ershov, H. C. Liu, L. Li, M. Buchanan, Z. R. Wasilewski, and V. Ryzhii, *Appl. Phys. Lett.* **70**, 1828 (1997).
- ¹¹X. Wu, E. S. Yang, and H. L. Evans, *J. Appl. Phys.* **68**, 2845 (1990).
- ¹²W. J. Moore, J. A. Freitas, and R. J. Molnar, *Phys. Rev. B* **56**, 12073 (1997).
- ¹³M. Sumiya, K. Yoshimura, K. Ohtsuka, and S. Fuke, *Appl. Phys. Lett.* **76**, 2098 (2000).
- ¹⁴V. Bougrov, M. Levinshtein, S. Rumyantsev, and A. Zubrilov, *Properties of Advanced Semiconductor Materials* (Wiley, New York, 2001).
- ¹⁵L. E. Byrum, G. Ariyawansa, R. C. Jayasinghe, N. Dietz, A. G. U. Perera, S. G. Matsik, I. T. Ferguson, A. Bezinger, and H. C. Liu, *J. Appl. Phys.* **105**, 023709 (2009).
- ¹⁶W. Gotz, N. M. Johnson, C. Chen, H. Liu, C. Kuo, and W. Imler, *Appl. Phys. Lett.* **68**, 3144 (1996).